Available online at www.sciencedirect.com

SciVerse ScienceDirect

Ceramics International 39 (2013) 6303–6311

CERAMICS INTERNATIONAL

www.elsevier.com/locate/ceramint

Study of AC electrical properties of V_2O_5–P_2O_5–B_2O_3–Dy_2O_3 glasses

R.V. Barde[a], S.A. Waghuley[b,*]

[a]Department of Engineering Physics, H.V.P.M. College of Engineering & Technology, Amravati 444 605, India
[b]Department of Physics, Sant Gadge Baba Amravati University, Amravati 444 602, India

Received 29 November 2012; received in revised form 16 January 2013; accepted 17 January 2013
Available online 31 January 2013

Abstract

The AC conductivity of glass samples of composition $60V_2O_5$–$5P_2O_5$–$(35-x)B_2O_3$–xDy_2O_3, $0.4 \le x \le 1.2$ has been analyzed. The samples were prepared by the usual melt-quench technique. The prepared compounds were analyzed by X-ray diffraction (XRD) and thermo gravimetric–differential thermal analysis (TG/DTA). The activation energies were evaluated using glass transition temperature (T_g) and peak temperature of crystallization (T_c) from TG/DTA. The dependence of activation energy on composition was discussed. The electrical conductance and capacitance were measured over a frequency range of 20 Hz to 1 MHz and a temperature range of 303–473 K; these reveal semiconducting features based predominantly on an ionic mechanism. The dielectric and complex-impedance response of the sample is discussed. The relaxation time was found to increase with increasing temperature. Jonscher's universal power law is applied to discuss the conductivity. The electrode polarization was found to be negligible and confirmed from electrical modulus.

Keywords: Complex impedance; Electrical conductance; Glasses

1. Introduction

During the last decades, many binary and ternary transition metal oxide (TMO) glasses have been studied because of their interesting semiconducting properties. Semiconducting behavior in these glasses is due to the hopping of 'polarons' from the higher to the lower valence states of the transition metal ions [1]. In these glasses the formation of small polarons are due to Strong electron–phonon interaction [2,3]. The V_2O_5 rich glasses in which V_2O_5 acts as the network former have the network structure mainly consisting of corner-sharing branched VO_4 tetrahedra. The reported network structure is made up of unaffected VO_5 groups as in vitreousV_2O_5 and affected VO_5 groups with alkaline earth ions in contrast to the vanadate glasses formed by conventional network formers in which only unaffected VO_5 groups are present [4]. These glasses are known to contain V^{4+} and V^{5+} ions where the electrical conduction was attributed to the hopping of $3d^1$ unpaired electron from V^{4+} to V^{5+} site, which induces a polarization of the vanadium ion around it and forms a polaron. The vanadate glasses have been received greater attention as a new branch in semiconducting glasses because of its wider glass-forming region in the phase diagram. This aspect possesses the possible technological applications in threshold switching, memory switching, electrical threshold, electrochemical batteries, and optical switching devices [5]. The electrical conductivity for such glasses depends strongly upon the local interaction of an electron with its surroundings and distance between vanadium ions [6–9].

B_2O_3 glasses are found to be very interesting amorphous materials whenever the specific structure and physical properties of which taken into consideration. In these glasses, two groups of bands are obtained: (i) due to trigonal BO_3 and (ii) due to the tetrahedral BO_4 units. By the addition of transition metal ions to the borate glasses, they would exhibit specific physical properties. When these glasses are grafted with alkaline earth ions, the resultant glasses are found to have several potential applications such as radiation dosimetry, phosphors, solar energy converters, vacuum ultraviolet optics and semiconductors lithography and in a number of electronic devices

*Corresponding author. Tel.: +91 94 23124882; fax: +91 72 1266 2135.
E-mail address: sandeepwaghuley@sgbau.ac.in (S.A. Waghuley).

0272-8842/$ - see front matter © 2013 Elsevier Ltd and Techna Group S.r.l. All rights reserved.
http://dx.doi.org/10.1016/j.ceramint.2013.01.054

[10–13]. Very few studies have been carried out on glasses containing B_2O_3 and V_2O_5. These glasses have their potential applications as optical and electrical memory switching, cathode materials for making solid devices and optical fiber [14].

The rare earth and transition metal containing glasses have been extensively studied using structural and optical spectroscopy due to their many potential applications. Some of the possible applications are optical amplifiers in telecommunication [15], phosphorescence materials and electrochemical batteries [16]. When rare earth metal ions added to the borate, they act as network modifiers and thus changes the properties of glasses. In rare earth metals, cerium oxide doped glasses have been studied by many researchers because of their applications as biosensor [17], photoluminescent material [18] and also used in tunable solid state lasers operating in the UV, violet and blue regions [19–21].

The aim of this work is to prepared the glasses with composition $60V_2O_5$–$5P_2O_5$–$(35-x)B_2O_3$–xDy_2O_3, $x=0.4$, 0.6, 0.8, 1 and 1.2 mol%. These glasses are studied by AC electrical and thermal properties. The characterization techniques, X-ray diffraction (XRD) and thermo gravimetric–differential thermal analysis (TG–DTA) are employed to study the structural properties of glass samples.

2. Experimental

2.1. Sample preparation

The glasses of the compositions of $60V_2O_5$–$5P_2O_5$–$(35-x)B_2O_3$–xDy_2O_3, $x=0.4$, 0.6, 0.8, 1 and 1.2 mol% were prepared by a conventional melt-quenching method. The AR grade (SD fine, India) chemicals were used in this investigation, which were weighed and mixed together. This mixture was homogenized and melted in silica crucible in a furnace at 1173 K for 3 h and the melt was stirred to remove CO_2. After melting, the mixture was poured onto a nonmagnetic stainless steel plate so that the sheet sample had a thickness of up to 3 mm. To avoid internal strains, the sample was annealed at 473 K for 1 h.

2.2. Materials characterizations

The sample was characterized by using XRD and TG–DTA techniques. The XRD pattern of powder sample was recorded on a XRD Philips PW 1830 using CuK_α radiation ($\lambda=1.54$ Å) in the range 20°–80°. The TG–DTA was carried out on Shimadzu DTG-60H thermal analyzer under nitrogen flow at the heating rate of 283 K/min. The temperature of the sample was varied from room temperature to 873 K. For the electrical measurements, the samples were polished and conducting silver paste was deposited on both sides. The sample area was taken to be the area exposed to the electrode surface. A firm contact was confirmed at the boundaries of the sample/electrode interfaces. The temperature dependence of AC conductivity (σ) and dielectric constant (ε') was measured by using LCR meter, Agilent Technology, Singapore. The operating voltage was 1 V. The Z and θ data can be read directly from the impedance meter in temperature range 303–473 K. The values of Z' and Z'' computed from $|Z|\cos\theta$ and $|Z|\sin\theta$, respectively. The capacitance (C) and the resistance (R) were read directly from the LCR meter, hence the real and imaginary parts of the dielectric constant (ε' and ε'') can be obtained. The measurements were performed in a frequency region of 20 Hz to 1 MHz and a temperature range of 303–473 K. The electrical modulus was studied for all compositions.

3. Result and discussion

3.1. XRD analysis

Fig. 1 depicts the XRD patterns of the $60V_2O_5$–$5P_2O_5$–$(35-x)B_2O_3$–xDy_2O_3, $x=0.4$, 0.6, 0.8, 1 and 1.2 mol%, pointed out the formation of glasses. There was no characteristic peak, which corresponds to any crystalline phase, and therefore it can be inferred that the obtained samples are amorphous. The amorphous hallow appears at the same 2θ-position.

3.2. Thermal analysis

TG–DTA analysis was carried out in order to study the changes occurred regarding the phase transition during heat treatment, from room temperature to 873 K in nitrogen atmosphere. TG/DTA studies are made to identify thermal stability of the $60V_2O_5$–$5P_2O_5$–$(35-x)B_2O_3$–xDy_2O_3 glass samples. TGA curves are displayed in Fig. 2(a and b). These curves show thermal dehydration in samples. The TGA curves shows 9% and 13% weight loss within the temperature range

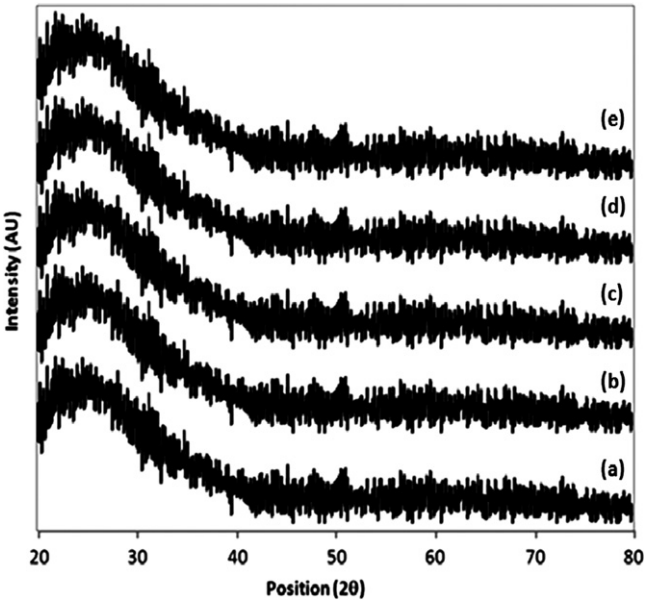

Fig. 1. XRD of $60V_2O_5$–$5P_2O_5$–$(35-x)B_2O_3$–xDy_2O_3 for: (a) $x=0.4$ mol%, (b) $x=0.6$ mol%, (c) $x=0.8$ mol%, (d) $x=1$ mol% and (e) $x=1.2$ mol%.

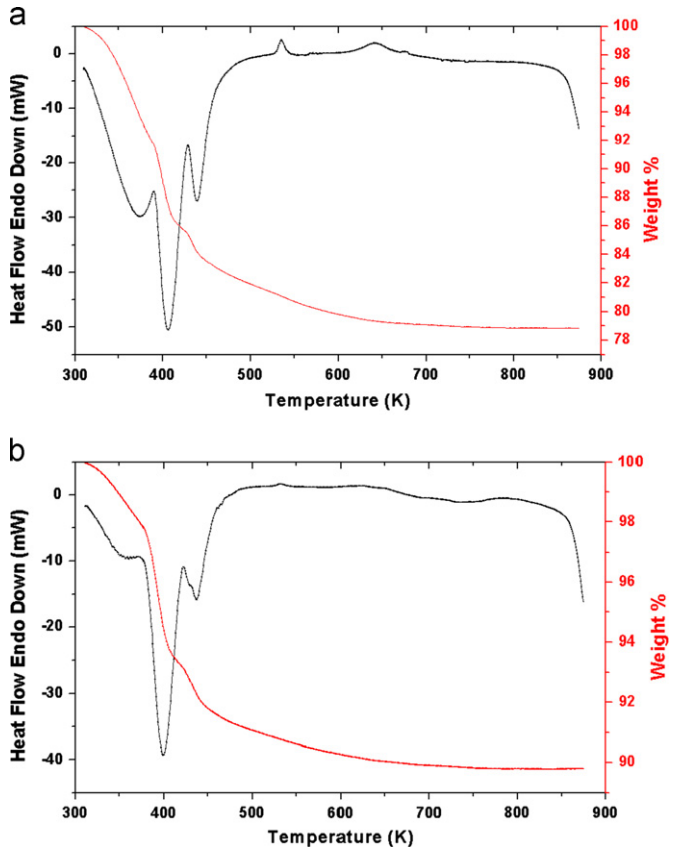

Fig. 2. TG–DTA Plot of: (a) $60V_2O_5$–$5P_2O_5$–$34.4B_2O_3$–$0.6Dy_2O_3$ and (b) $60V_2O_5$–$5P_2O_5$–$33.8B_2O_3$–$1.2Dy_2O_3$.

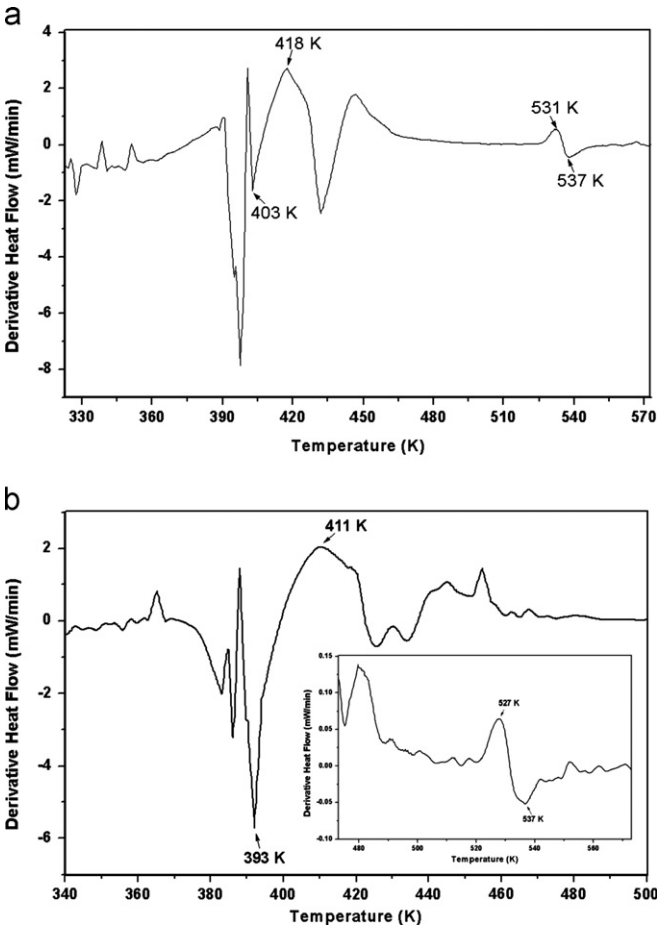

Fig. 3. Simultaneous recorded DDTA curve of: (a) $60V_2O_5$–$5P_2O_5$–$34.4B_2O_3$–$0.6Dy_2O_3$ and (b) $60V_2O_5$–$5P_2O_5$–$33.8B_2O_3$–$1.2Dy_2O_3$.

of 303–473 K, which assign to the loss of water molecules for 0.6 mol% and 1.2 mol% of Dy_2O_3. After which a gradual weight loss is observed till ~573 K. This may be due to the condensation of structural hydroxyl groups.

Fig. 2(a and b) shows the DTA profiles of the glasses $60V_2O_5$–$5P_2O_5$–$(35-x)B_2O_3$–xDy_2O_3 for $x=0.6$ and 1.2. The large endothermic peak appears between 393 and 413 K, followed by small exothermic peak between 523 and 573 K, respectively. Each peak is attributed to glass transition temperatures (T_g) and crystallization temperatures (T_c), respectively, from which the T_g and T_c were estimated. It can be seen that T_c decreased gradually with the increasing 'x', suggesting that the crystallization of the glasses becomes easy. The T_g of the glasses were 407 and 399 K for the sample $60V_2O_5$–$5P_2O_5$–$34.4B_2O_3$–$0.6Dy_2O_3$ and $60V_2O_5$–$5P_2O_5$–$33.8B_2O_3$–$1.2Dy_2O_3$ whereas, T_c of the glasses were 535 and 531 K, respectively. This difference may attribute to different annealing conditions adopted. The thermal stability (T_c–T_g) of glasses was decrease with increasing Dy_2O_3. The thermal stability of the glass was found to be excellent for the composition with $x=0.6$.

The DTA curve and its derivatives (DDTA) are simultaneously recorded as shown in Fig. 3(a and b), the two inflection points that is maximum and minimum slops of the DTA peak corresponds to maximum and minimum of the DDTA double peaks are obtained. Therefore the temperature Tf_1 and Tf_2 corresponding to endothermic and exothermic peaks can be easily and exactly detected on DDTA curve. The activation energy (E_a) of first order reaction using temperature of two inflection points Tf_1 and Tf_2 was derived from Eq. (1). The endo and exo activation energy were found to be 20.05 kJ/g-mol and 181.123 kJ/g-mol, respectively, for the sample $60V_2O_5$–$5P_2O_5$–$34.4B_2O_3$–$0.6Dy_2O_3$ whereas for the sample $60V_2O_5$–$5P_2O_5$–$33.8B_2O_3$–$1.2Dy_2O_3$ were found to be 14.68 kJ/g-mol and 107 kJ/g-mol, respectively [22].

$$\frac{E_a}{R}\left(\frac{1}{Tf_1}-\frac{1}{Tf_2}\right)=1.92 \quad (1)$$

where R is universal gas constant.

3.3. Electrical conductivity measurements

Complex impedance measurements were carried out to determine the electrical conductivity and the AC behavior of glasses over a range of temperature and frequencies. The temperature-dependent impedance data of all the compositions have been analyzed. Fig. 4 shows the impedance plot (Z' vs. Z'') obtained for 1.2 mol% of Dy_2O_3 doped composition at different temperatures. Such shapes are

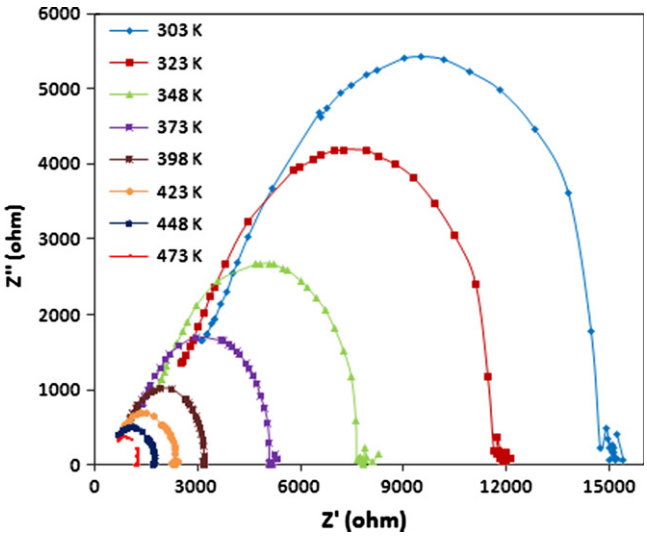

Fig. 4. Cole–cole plot of $60V_2O_5$–$5P_2O_5$–$33.8B_2O_3$–$1.2Dy_2O_3$.

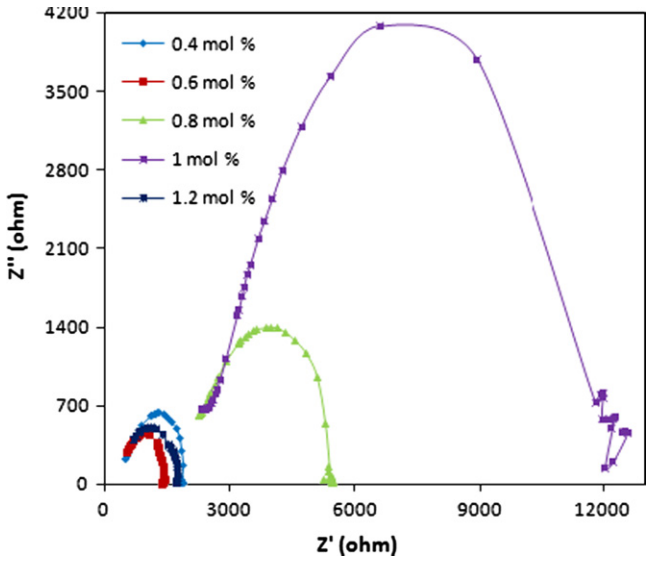

Fig. 5. Cole–cole plot of $60V_2O_5$–$5P_2O_5$–$(35-x)B_2O_3$–xDy_2O_3 at 448 K.

typically observed in superionic solids exhibiting lattice disorder [23]. The center of semicircle was found bellow Z' axis. This behavior shows that the nature of relaxation of ions is non-Debye. As the temperature increases, the radius of the semicircle decreases, which shows an activated conduction mechanism [24].

The impedance shows a low frequency spike and a small portion of the semicircle. The semicircle at the high frequency and low frequency region is due to the bulk relaxation and interfacial effects respectively. Semicircle was successfully fitted using parallel RC circuit. Fig. 5 shows the impedance plot for all samples at 448 K, which exhibited same behavior. From the semicircle the associate value of capacitance (C) determine by using the relation $2\pi fRC=1$. Here R is the value of real part of impedance at the top of semicircle [25–28]. The value of R and C of parallel RC circuit for different temperature are listed in Table 1. The relaxation time of samples were calculated by using the relation $\omega\tau=1$. The plot of relaxation time against inverse of temperature is as shown in Fig. 6 for $x=1.2$. It is found that the relaxation time obeys the Arrhenius relation

$$\tau = \tau_0 \exp\left(\frac{E_\tau}{KT}\right) \tag{2}$$

where E_τ is the activation energy. From the activation energy we can predict that relaxation time is determined by the flow of charge carriers. It is cleared that the conductivity is influence by both frequency and temperature and AC conductivity may due to the polaron hopping mechanism [29,30].

The dc-resistance of the samples was obtained from the intersection of the semicircle with the real axis at low frequency. With increasing temperature, intercepts of the semicircle shift toward the origin. The dc-conductivity (σ_{dc}) was calculated using sample dimensions. The value of conductivity shall be increases with temperature. This means that the bulk resistance of sample is decreased. This gradual enhancement in conductivity is due to activated conduction mechanism. The reciprocal temperature dependence of the dc conductivity is shown in Fig. 7. This plot shows that the dc conductivity exhibits an Arrhenius-type temperature dependence given by the relation

$$\sigma_{dc} = \sigma_0 \exp\left(-\frac{E_{dc}}{KT}\right) \tag{3}$$

The E_{dc} was calculated from the least square straight-line fitting. The values of E_{dc} for all compositions at room temperature are given in Table 1. It is observed that the conductivity shows a random nature. It is maximum for 0.6 mol% of Dy_2O_3 and decreases for 0.8 and 1 mol% of Dy_2O_3. If we further increase the mol% of Dy_2O_3 the conductivity increases. The maximum in conductivity corresponds with minimum of activation energy. This could be explained on the basis of Mixed Glass Former effect [31]. The increase in conductivity explains on the basis of the Anderson and Stuart model. In present case, Dy being slightly larger in size than boron, the substitution of Dy in place of boron will increase the interionic bond distance. Thus with the addition of 0.4 mol% Dy_2O_3, the structure becomes loose and hence the conductivity increases [32]. The decrease in conductivity beyond 0.8 mol% Dy_2O_3 may be due to elimination of the non-bridging oxygen's (NBOs) and simultaneously creates bridging oxygen's (BOs) [33].

Fig. 8 depicts frequency dependent conductivity plot of $\log(\omega)$ versus $\log(\sigma)$ for the composition $60V_2O_5$–$5P_2O_5$–$33.8B_2O_3$–$1.2Dy_2O_3$ at various temperatures. In low frequency region the conductivity is found to be almost frequency independent, suggesting that the ionic diffusion is random less via activated hopping process. At high frequency region, dispersion in conductivity has been observed. This dispersion is largest at lower temperatures.

Table 1
DC conductivity (σ_{dc}), activation energy (E_{dc}), R_{max}, C and relaxation time (τ).

Sample mol% of Dy_2O_3	σ_{dc} at 303 K (S cm^{-1})	σ_{dc} at 473 K (S cm^{-1})	E_{dc} (eV)	R_{max} at 303 K (Ω)	C at 303 K (F)	τ at 303 K (s)
0.4	6.2×10^{-5}	6.17×10^{-4}	0.173	9619.55	1.09×10^{-9}	1.05×10^{-7}
0.6	9.17×10^{-5}	1.31×10^{-3}	0.20	11612.41	9.06×10^{-10}	1.05×10^{-7}
0.8	6.08×10^{-5}	3.82×10^{-4}	0.27	31069.52	3.38×10^{-10}	2.78×10^{-7}
1	4.7×10^{-5}	2.17×10^{-4}	0.24	18919.50	2×10^{-11}	3.78×10^{-7}
1.2	1.07×10^{-4}	1.33×10^{-3}	0.19	9542.67	3.30×10^{-10}	3.15×10^{-7}

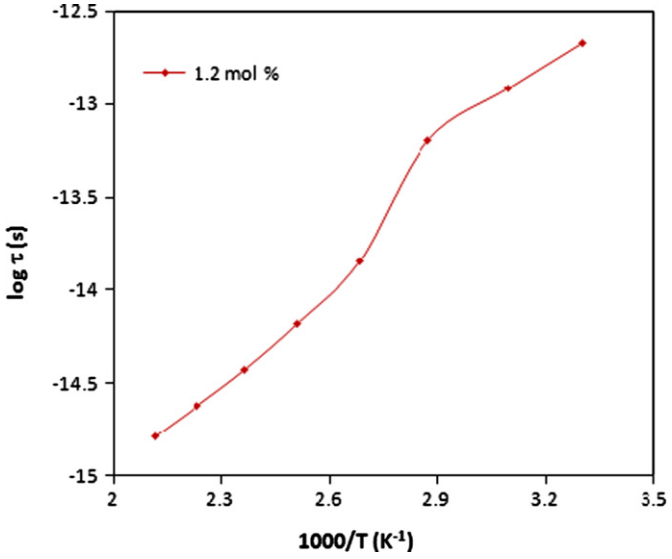

Fig. 6. Plot between relaxation time and inverse of temperature for $60V_2O_5$–$5P_2O_5$–$33.8B_2O_3$–$1.2Dy_2O_3$.

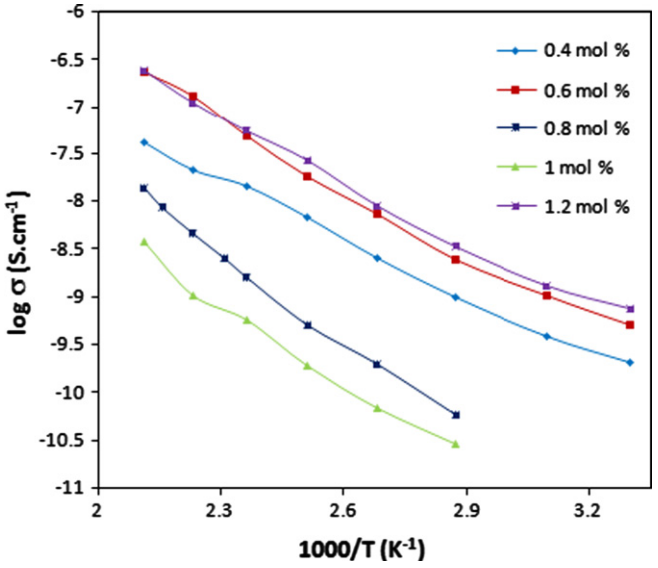

Fig. 7. Temparatrure dependent DC conductivity of $60V_2O_5$–$5P_2O_5$–$(35-x)B_2O_3$–xDy_2O_3.

It is seen from the Fig. 8 that, as the temperature increases, the frequency at which the dispersion becomes large, shifts to higher frequency region, which is analyzed by using

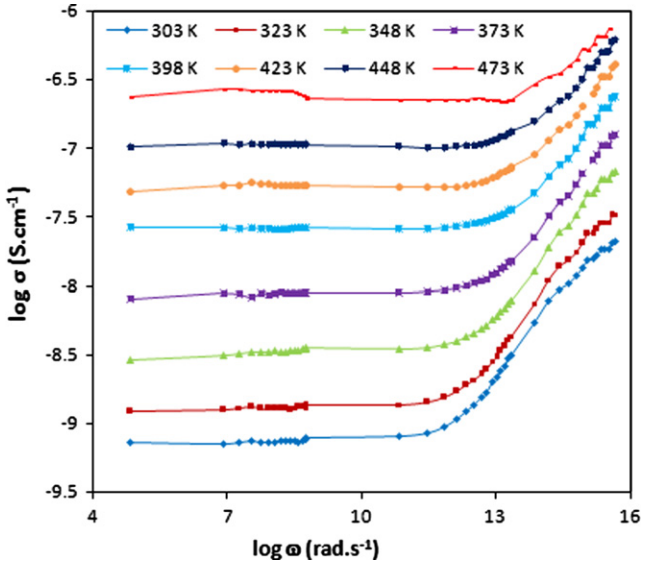

Fig. 8. Frequency-dependent conductivity plot of $60V_2O_5$–$5P_2O_5$–$33.8B_2O_3$–$1.2Dy_2O_3$.

Jonscher's universal power law [34,35].

$$\sigma(\omega) = \sigma(0) + A\omega^n = \sigma(0)\left[1 + \left(\frac{\omega}{\omega_P}\right)\right]^n \quad (4)$$

where $\sigma(0)$ is the frequency-independent dc conductivity of the sample, ω_P hopping frequency, A is a weak temperature-dependent quantity and n is the power law exponent. The conductivity data of all glass composition have been fitted to the above equation (Eq. (4)). shows good agreements with the experimental data.

Fig. 9 shows the plots of Z'' as a function of frequency at different temperatures, which shows non-Debye-type peaks. This may be due to the existence of distributed relaxation time. With the increase in temperature, peak maxima (ω_m) are found to shift toward high frequency region. The above shift obeys the Arrhenius equation, which suggests that the ion transport follows the hoping mechanism [24].

The variation of Z' with frequency for various temperatures is shown in Fig. 10. It is observed that the value of Z' is constant for lower frequency at all temperature and decreases with increase in frequency and temperature. This decrease in Z' suggests an increase in AC conductivity of the material with increase in frequency and temperature. The Z'

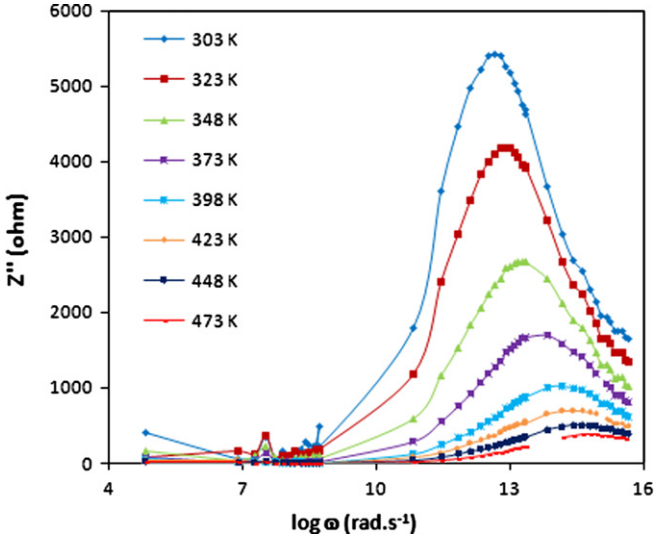

Fig. 9. Plot of Z'' as a function of frequency.

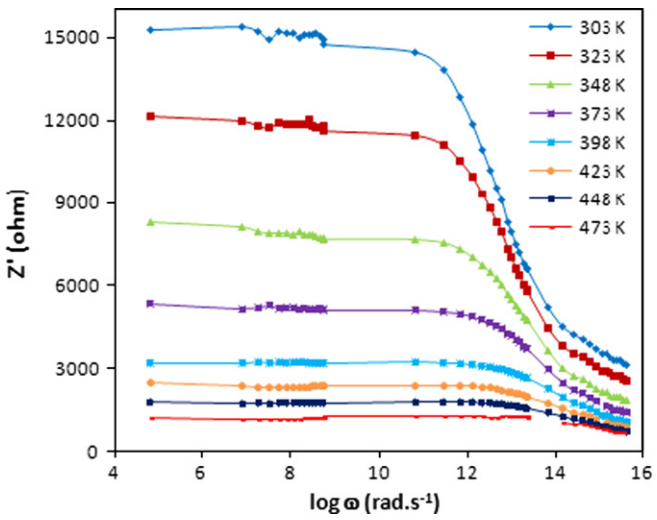

Fig. 10. Plot of Z' as a function of frequency.

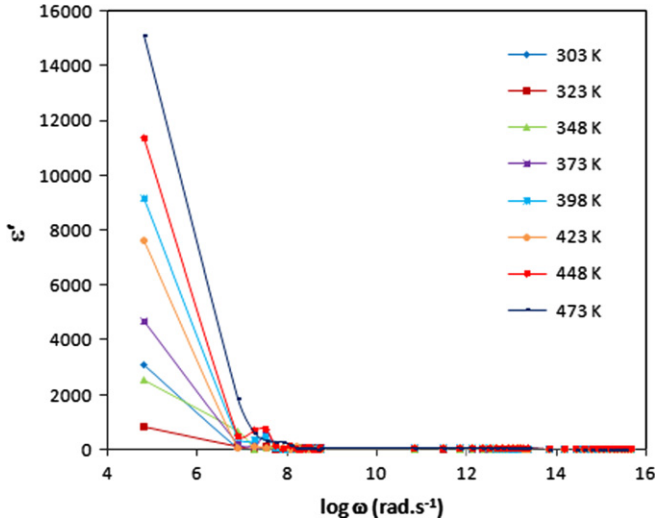

Fig. 11. Frequency dependence plot of real part of dielectric constant.

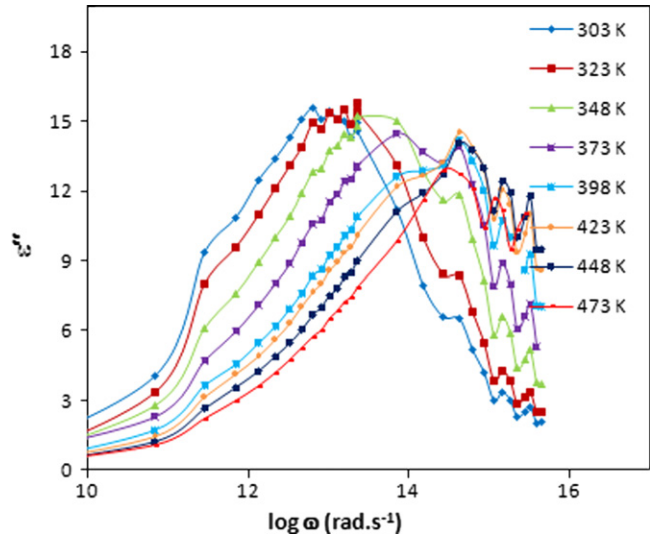

Fig. 12. Frequency dependence plot of imaginary part of dielectric constant.

values fuse at higher frequency for all temperature, which is due to the release of space charge and reduction in potential barrier of the material with increase in temperature [36].

Fig. 11 shows the frequency dependence plots of real part of dielectric constant ε' at various temperatures for glass composition $60V_2O_5$–$5P_2O_5$–$33.8B_2O_3$–$1.2Dy_2O_3$. It is found that at a particular temperature the value of ε' decreases with increasing frequency. This shows that the contribution from charge carriers decreases with increasing frequency and attains a constant value ε'_∞, which may be due to the effect of much more rapid polarization process in the sample. In low frequency region, the value of ε' is high due to the presence of metallic or blocking electrodes, which accumulates charge at the electrode-sample interface. In the high frequency region, at low temperatures, the well-known non-Debye behavior is observed [37–41].

Fig. 12 shows the frequency dependence plots of imaginary part of dielectric constant ε'' at various temperatures for glass composition $60V_2O_5$–$5P_2O_5$–$33.8B_2O_3$–$1.2Dy_2O_3$. In this figure it is observed that the ε'' exhibit the loss peak in the high frequency region, which may be due to the polarization of the samples. This obeys the Debye model [42]. We found that the temperature dependence of dielectric relaxation peak (ω_m) obeys a simple Arrhenius behavior with the same activation energy as dc conductivity. The correlation between the electrical conductivity, σ_{dc}, and ω_m of dielectric relaxation peak can be described by the Barton, Nakajima, Namikawa (BNN). The dielectric relaxation in glasses may be due to the hopping mechanism of charge carrier transport [43].

The dielectric loss tanδ shows that the phase difference is due to the loss of energy within the sample at a definite

frequency. The frequency dependence of tanδ at different temperatures for the glass composition $60V_2O_5$–$5P_2O_5$–$33.8B_2O_3$–$1.2Dy_2O_3$ is shown in Fig. 13. At lower frequencies, tanδ increases with increase in frequency and shows a peak at particular frequency. This may be due to rapid response of active component than its reactive component. At higher frequencies, tanδ decreases owing to the reactive component response to the frequency whereas the current due to the active component is independent of frequency [44]. With increasing temperature the tan δ peak shifts to higher frequency. This dependence of tan δ on frequency is related with losses by conduction [41]. The observed dielectric loss may be due to two reasons: (i) the thermal excitation generates the Debye-type freely rotating dipoles and (ii) at higher temperatures, electrons take part in conduction scattered by phonon [45].

3.4. Electric modulus

The electric modulus is an alternative approach to investigate the complex electrical response of material, which nullify the electrode polarization effect. Fig. 14 shows the dependence of real part of the modulus (M') on log (ω) for the composition $60V_2O_5$–$5P_2O_5$–$33.8B_2O_3$–$1.2Dy_2O_3$ at different temperatures. At higher frequencies, M' reaches a maximum constant value and at low frequencies M' approaches to zero indicates that the electrode polarization makes a negligible contribution. The dispersion in between these frequencies is due to the conductivity relaxation [39,46].

Fig. 15 represent the variation of imaginary part of electric modulus (M'') with log (ω) at different temperatures for the composition $60V_2O_5$–$5P_2O_5$–$33.8B_2O_3$–$1.2Dy_2O_3$. It is observed that the shape of each curve is non-Lorentzian type and with the increase in temperature, the peak frequency shifts toward the higher frequency region. It may be due to the distribution of attempt frequencies to penetrate the potential barrier [24,39,46].

Fig. 16 represent the plot of M' and M'' for the composition $60V_2O_5$–$5P_2O_5$–$33.8B_2O_3$–$1.2Dy_2O_3$ at different temperatures, which shows the semi-arc with the center under the M' axes. This may be due to the existence of a distribution of some physical characteristic of the material. This phenomenon is studied using a electronic circuit where a constant phase element is used. The impedance of this element is given by Eq. (5) [47]

$$\frac{1}{Z_{CPE}} = Y_0(j\omega)^{\beta} \tag{5}$$

where Y_0 is the admittance ($1/|Z|$) and β is a value between 0 and 1.

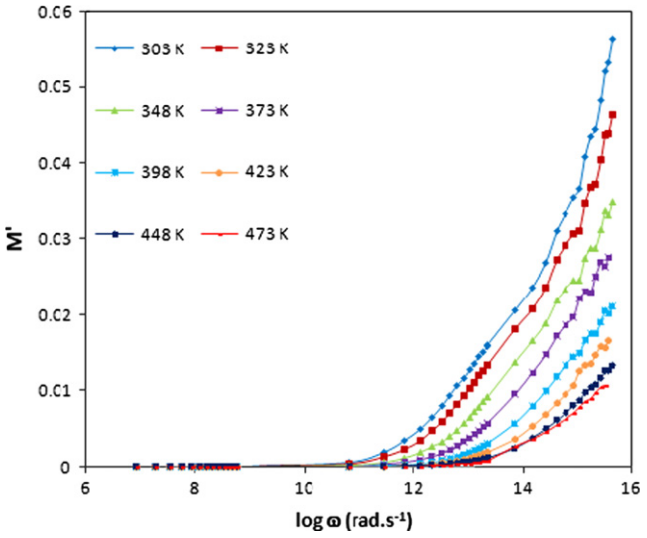

Fig. 14. Real part of the modulus vs. log (ω) for the composition $60V_2O_5$–$5P_2O_5$–$33.8B_2O_3$–$1.2Dy_2O_3$.

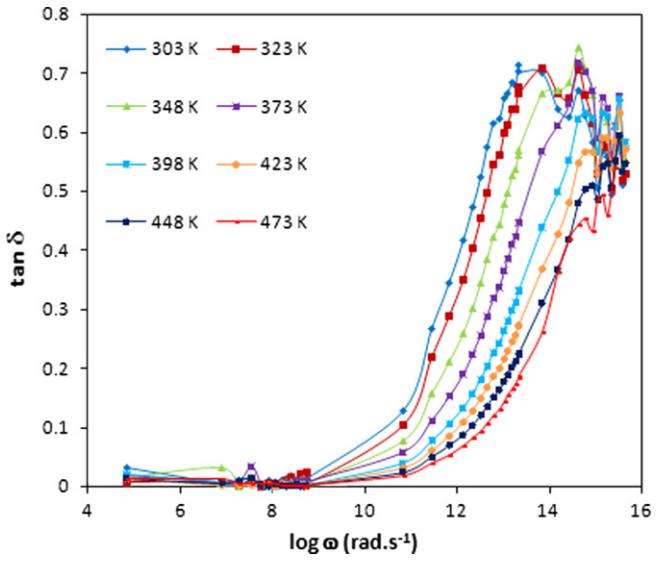

Fig. 13. Plot of dielectric loss vs. log (ω) for $60V_2O_5$–$5P_2O_5$–$33.8B_2O_3$–$1.2Dy_2O_3$.

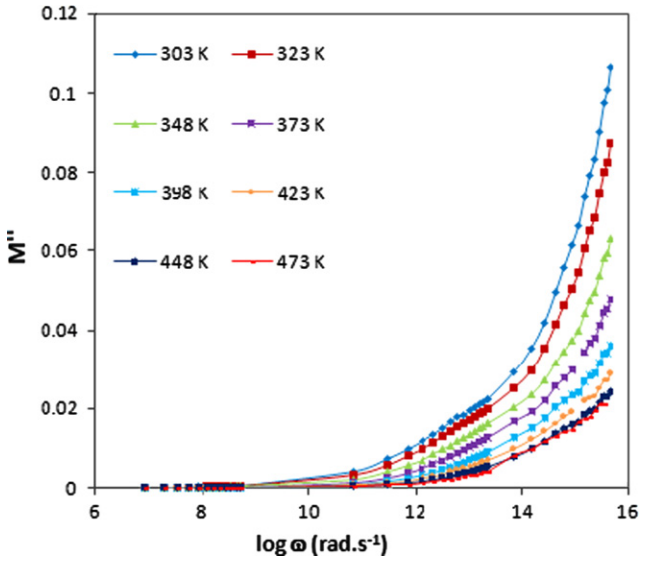

Fig. 15. Imaginary part of the modulus versus log (ω) for the composition $60V_2O_5$–$5P_2O_5$–$33.8B_2O_3$–$1.2Dy_2O_3$.

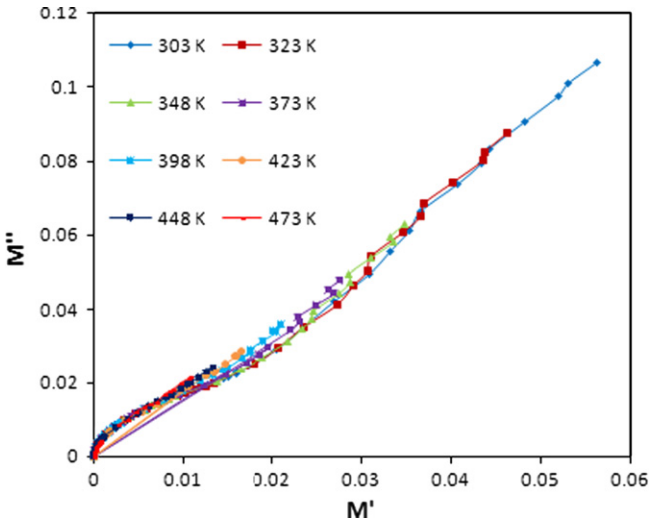

Fig. 16. Nyquist plot of electrical modulus for $60V_2O_5$–$5P_2O_5$–$33.8B_2O_3$–$1.2Dy_2O_3$.

4. Conclusions

The preparation of the conducting glasses by melt-quenching technique is a very simple. The amorphous nature of glasses was reflected from XRD study. The glass transition temperature (T_g) was observed to be decreases with Dy_2O_3 content. The thermal stability was found to be excellent for the composition $60V_2O_5$–$5P_2O_5$–$34.4B_2O_3$–$0.6Dy_2O_3$. The AC conductivity obeys a power law. The semicircular behavior of Z' and Z'' suggest that the conduction through ionic mechanism, predominantly operating at the grain surface. The results indicate that at the highest temperature, the sample is more conductive. The relaxation times for the sample obtained at different temperatures follow the changes in sample resistivity. The dielectric constant of the sample was decreases with increasing frequency and increases with increasing temperature. The electrical modulus study revels that the electrode polarization has negligible contribution. The tanδ peak shifts to higher frequency with increasing temperature. The tanδ peak is positioned at low frequency region, where the conductivity is dominated by DC conductivity.

Acknowledgment

Authors are thankful to Head, Department of Physics Sant Gadge Baba Amravati University, Amravati for providing necessary facilities.

References

[1] A. Al- Hajry, A.A. Soliman, M.M. El-Desoky, Electrical and thermal properties of Fe_2O_3–Bi_2O_3–$Na_2B_4O_7$ glasses, Thermochimica Acta 427 (2005) 181–186.

[2] M.M. El-Desoky, A. Al- Shahrani, Variable range hopping in $Fe_2O_3Bi_2O_3$–$K_2B_4O_7$ glasses, Journal of Materials Science: Materials in Electronics 16 (2005) 221–224.

[3] A. Al-Hajry, N. Tashtoush, M.M. El-Desoky, Characterization and transport properties of semiconducting Fe_2O_3–Bi_2O_3–$Na_2B_4O_7$ glasses, Physica B 368 (2005) 51–57.

[4] S. Sen, A. Ghosh, Ac conductivity of strontium vanadate semiconducting glasses, Journal of Physics: Condensed Matter 13 (2001) 1979–1984.

[5] Y.B. Saddeek, E.R. Shaaban, K.A. Aly, I.M. Sayed, Characterization of some lead vanadate glasses, Journal of Alloys and Compounds 478 (2009) 447–452.

[6] M.M. El-Desoky, Small polaron transport in V_2O_5–NiO–TeO_2 glasses, Journal of Materials Science: Materials in Electronics 14 (2003) 215–221.

[7] A. Al-Shahrani, A. Al-Hajry, M.M. El-Desoky, Non-adiabatic small polaron hopping conduction in sodium borate tungstate glasse, Physica Status Solidi 300 (2003) 378–387.

[8] M.M. El-Desoky, N.M. Tashtoush, M.H. Habib, Characterization and electrical properties of semiconducting Fe_2O_3–Bi_2O_3–$K_2B_4O_7$ glasses, Journal of Materials Science: Materials in Electronics 16 (2005) 533.

[9] M.M. El-Desoky, A. Al-Hajry, M. Tokunaga, T. Nishida, M.Y. Hassaan, Effect of sulfur addition on the redox state of iron in iron phosphate glasse, Hyperfine Interactions 156–157 (2004) 547–553.

[10] A. Terczynska-Madej, K. Cholewa-Kowalska, M. Laczka, The effect of silicate network modifiers on colour and electron spectra of transition metal ions, Optical Materials 32 (2010) 1456–1462.

[11] P. Venkat Reddy, C. Laxmi kanth, V. Prasanth Kumar, N. Veeraiah, P. Kistaiah, Optical and thermoluminescence properties of R_2O–RF–B_2O_3 glass systems doped with MnO, Journal of Non-Crystalline Solids 351 (2005) 3752–3759.

[12] A.Ramesh Babu, Ch. RajyaSree, P. Srinivasa Rao, P.M. Vinaya Teja, D. Krishna Rao, Vanadyl ions influence on spectroscopic and dielectric properties of glass network, Journal of Molecular Structure 1005 (2011) 83–90.

[13] A. Ramesh Babu, Ch. RajyaSree, P.M. Vinaya Teja, S. Yusub, D. Krishna Rao, Influence of manganese ions on spectroscopic and dielectric properties of LiF–SrO–B_2O_3 glasses, Journal of Non-Crystalline Solids 358 (2012) 1391–1398.

[14] G.D. Khattak, A. Mekki, Structure and electrical properties of SrO–borovanadate $(V_2O_5)_{0.5}(SrO)_{0.5-y}(B_2O_3)_y$ glasses, Journal of Physics and Chemistry of Solids 70 (2009) 1330–1336.

[15] W.A. Pisarski, T. Goryczka, B. Wodecka-Dus, M. Plonska, J. Pisarska, Structure and properties of rare earth-doped lead borate glasses, Materials Science and Engineering B 122 (2005) 94–99.

[16] J. Qiu, H. Igarashi, A. Makishima, Long-lasting phosphorescence in Mn^{2+}: Zn_2GeO_4 crystallites precipitated in transparent GeO_2–B_2O_3–ZnO glass–ceramics, Science and Technology of Advanced Materials 6 (2005) 431–434.

[17] A.A. Ansari, A. Kaushik, P.R. Solanki, B.D. Malhotra, Sol–gel derived nanostructured cerium oxide film for application to cholesterol biosensor, Electrochemistry Communications 10 (2008) 1246–1268.

[18] H. Guo, Y. Qiao, Preparation, structural and photoluminescent properties of CeO_2:Eu^{3+} films derived by Pechini sol–gel process, Applied Surface Science 254 (2008) 1961–1965.

[19] T. Murata, M. Sato, H. Yoshida, K. Morinaga, Compositional dependence of ultraviolet fluorescence intensity of Ce^{3+} in silicate, borate, and phosphate glasses, Journal of Non-Crystalline Solids 351 (2005) 312–316.

[20] M. Laroche, S. Girard, R. Moncorge, M. Bettinelli, R. Abdulsabirov, V. Semashko, Beneficial effect of Lu^{3+} and Yb^{3+} ions in UV laser materials, Optical Materials 22 (2003) 147–154.

[21] G. PalSingh, D.P. Singh, Spectroscopic study of ZnO doped CeO_2–PbO–B_2O_3 glasses, Physica B 406 (2011) 3402–3405.

[22] S.A. Waghuley, Synthesis, characterization CO_2 gas sensing response of SnO_2/Al_2O_3 doubled layered sensor, Indian Journal of Pure and Applied Physics 49 (2011) 816–819.

[23] A. Viswanathan, S.A. Suthanthiraraj, B.V.R. Chowdari, Impedance and modulus spectra of the fast ion conducting system CuI–Ag_2WO_4, Solid State Ionics—Materials and Applications (1992) 379–383.

[24] A. Bhide, K. Hariharan, Sodium ion transport in $NaPO_3$–Na_2SO_4 glasses, Materials Chemistry and Physics 105 (2007) 213–221.
[25] C.J. Lio, B.V.R. Chowdari, G.V. Subba Rao, J.L. Souquet, Lithium conducting glass ceramic with Nasicon structure, Materials Research Bulletin 37 (2002) 1419–1430.
[26] P. Kluvanek, R. Klement, M. Karacon, Investigation of the conductivity of the lithium borosilicate glass system, Journal of Non-Crystalline Solids 353 (2007) 2004–2007.
[27] X. Xu, Z. Wen, Z. Gu, X. Xu, Z. Lin, Lithium ion conductive glass ceramics in the system $Li_{1.4}Al_{0.4}(Ge_{1-x}Ti_x)_{1.6}(PO_4)_3$ ($x=0$–1.0), Solid State Ionics 171 (2004) 207–213.
[28] K. Shrinivas, P. Sarah, S.V. Suryanarayana, Impedance spectroscopy study of polycrystalline $Bi_6Fe_2Ti_3O_{18}$, Bulletin of Material Science 26 (2003) 247–253.
[29] S.K. Deshpande, V.K. Shrikhande, M.S. Jogad, P.S. Goyal, G.P. Kothiyal, Conductivity studies of lithium zinc silicate glasses with varying lithium contents, Bulletin of Material Science 30 (2007) 497–502.
[30] K.P. Padmasree, D.K. Kanchan, Conductivity and dielectric studies on $20CdI_2$–$80[xAg_2O-y(0.7V_2O_5$–$0.3B_2O_3)]$ super ion conducting system where $1 \le x/y \le 3$, Journal of Non-Crystalline Solids 352 (2006) 3841–3848.
[31] V.K. Deshpande, A. Pradel, M. Ribes, The mixed glass former effect in the Li_2S:SiS_2:GeS_2 system, Materials Research Bulletin 23 (1988) 379–384.
[32] R.S. Gedam, V.K. Deshpande, An anomalous enhancement in the electrical conductivity of Li_2O: B_2O_3: Al_2O_3 glasses, Solid State Ionics 177 (2006) 2589–2592.
[33] M.N. Alexander, P.I.K. Onorato, C.W. Struck, J.R. Rozen, G.W. Tasker, D.R. Uhlmann, Structure of alkali (alumino)silicate glasses: I. Tl^+ luminescence and the nonbridging oxygen issue, Journal of Non-Crystalline Solids 79 (1986) 137–154.
[34] A.K. Jonscher, The 'universal' dielectric response, Nature 267 (1977) 673–679.
[35] C.R. Mariappan, G. Govindaraj, S.Vinoth Rathan, G.Vijaya Prakash, Preparation, characterization, ac conductivity and permittivity studies on vitreous $M_4AlCdP_3O_{12}$ (M=Li, Na, K) system, Materials Science and Engineering B 121 (2005) 2–8.
[36] S.K. Bera, S.K. Barik, R.N.P. Choudhary, P.K. Bajpai, Electrical and magnetic properties of $(BiNa)_{1/2}(FeV)_{1/2}O_3$, Bulletin of Material Science 35 (2012) 47–51.
[37] A.K. Jonscher, Dielectric Relaxation in Solids, Chelsea Dielectric Press, London, 1983.
[38] J.R. Macdonald, Impedance Spectroscopy, Wily, New York, 1987.
[39] A. Dutta, T.P. Sinha, P. Jena, S. Adak, Ac conductivity and dielectric relaxation in ionically conducting soda–lime–silicate glasses, Journal of Non-Crystalline Solids 354 (2008) 3952–3957.
[40] S. Jayaseelan, P. Muralidharan, M. Venkateswarlu, N. Satyanarayana, Ion transport and relaxation studies of silvervanadotellurite, Materials Chemistry and Physics 87 (2004) 370–377.
[41] S. Vinoth Rathan, G. Govindaraj, Thermal and electrical relaxation studies in $Li_{(4+x)}Ti_xNb_{1-x}P_3O_{12}$ ($0.0 \le x \le 1.0$) phosphate glasses, Solid State Sciences 12 (2010) 730–735.
[42] F.A.A. Wahab, M.A. Baki, Electrical conduction and dielectric properties of lithium aluminum silicate glasses doped with Cr^{3+} ions, Journal of Non-Crystalline Solids 355 (2009) 2239–2249.
[43] L. Murawski, R.J. Barczynski, Electronic and ionic relaxations in oxide glasses, Solid State Ionics 176 (2005) 2145–2151.
[44] S. Chopra, S. Sharma, T.C. Goel, R.G. Mendiratta, Structural, dielectric and pyroelectric studies of Pb_{1-x} Ca_x TiO_3 thin films, Solid State Communications 127 (2003) 299.
[45] E.E. Shaishay, F. El-Desouki, I. Shaltout, A.A. Bahgat, Electrical relaxation in mixed alkali Bi_2O_3–K_2O–Li_2O–Fe_2O_3 glasses, Journal of Materials Science & Technology 22 (2006) 701–707.
[46] S. Bhattacharya, A. Ghosh, Conductivity relaxation in some fast ion-conducting AgI–Ag_2O–V_2O_5 glasses, Solid State Ionics 161 (2003) 61–65.
[47] M.P.F. Grac, M.A. Valent, M.G.Ferreira da Silva, Electrical properties of lithium niobium silicate glasses, Journal of Non-Crystalline Solids 325 (2003) 267–274.